Millimeter-Wave NOMA Transmission in Cellular M2M Communications for Internet of Things

Tiejun Lv, *Senior Member, IEEE*, Yuyu Ma, Jie Zeng, *Senior Member, IEEE*, and P. Takis Mathiopoulos, *Senior Member, IEEE*

***Abstract*—Massive connectivity and low latency are two important challenges for the Internet of Things (IoT) to achieve the quality of service provisions required by the numerous devices it is designed to service. Motivated by these challenges, in this paper we introduce a new millimeter-wave nonorthogonal multiple access (mmWave-NOMA) transmission scheme designed for cellular machine-to-machine (M2M) communication systems for IoT applications. It consists of one base station (BS) and numerous multiple machine type communication (MTC) devices operating in a cellular communication environment. We consider its down-link performance and assume that multiple MTC devices share the same communication resources offered by the proposed mmWave-NOMA transmission scheme, which can support massive connectivity. For this system, a novel MTC pairing scheme is introduced the design of which is based upon the distance between the BS and the MTC devices aiming at reducing the system overall overhead for massive connectivity and latency. In particular, we consider three different MTC device pairing schemes, namely: 1) random near and the random far MTC devices; 2) nearest near and the nearest far MTC devices (NNNF); and 3) nearest near and the farthest far MTC device. For all three pairing schemes, their performance is analyzed by deriving closed-form expressions of the outage probability and the sum rate. Furthermore, performance comparison studies of the three MTC device pairing schemes have been carried out. The validity of the analytical approach has been verified by means of extensive computer simulations. The obtained performance evaluation results have demonstrated that the proposed cellular M2M communication system employing the mmWave-NOMA transmission scheme improves outage probability as compared to equivalent systems using mmWave with orthogonal multiple access schemes.**

***Index Terms*—Internet of Things (IoT), machine type communication (MTC) device pairing schemes, machine-to machine (M2M), millimeter-wave nonorthogonal multiple access (mmWave-NOMA), outage probability.**

I. Introduction

THROUGH the development of numerous applications, the Internet of Things (IoT) [1], [2] aims at providing a host of new services to citizens, private and public companies as well as to governmental administrations [3]–[5]. In general, it is envisioned that the IoT will provide a platform which will connect a huge number of devices in order to gather, share, and forward information between devices as well as their users [6]–[8]. It is estimated that by the year 2020 almost 50 billion of devices will connected to this platform [9]. To accommodate the drastically increasing number of these devices, the resulting huge increase in data traffic will have a great impact on the design and implementation of fifth generation (5G) wireless communication systems. In particular, there will be challenging requirements for their efficient operation, including massive connectivity and low latency [10], [11]. On the one hand, machine-to-machine (M2M) communications have been regarded as one of the promising new technologies to realize IoT employing the 5G network [12]. M2M communication systems realize automated data communications among machine type communication (MTC) devices thus constituting the basic communication infrastructure for the emerging IoT [13], [14]. In addition, long term evolution (LTE) for MTC and narrow band IoT have been proposed on top of existing cellular standards, which can provide reliable solutions for M2M communications [15]. On the other hand, nonorthogonal multiple access (NOMA), which has been proposed as a multiple access scheme to be employed with 5G wireless communication systems, has the ability to support massive connectivity by means of nonorthogonal resource allocation while simultaneously reducing latencies by its grant-free scheduling. For example, in [16], an interesting power-domain user multiplexing scheme for future radio access has been proposed. Note that, in conjunction with NOMA transmission, the joint use of superposition code at the transmitter and successive interference cancellation (SIC) at the receiver has been also studied [16]–[20].

As opposed to orthogonal multiple access (OMA) schemes, NOMA can support a large number of users via nonorthogonal resource allocation, through the simultaneous use of the time, frequency, and code domains as well as well as multiplexing them at different power levels [21]–[23]. For example, under poor channel conditions, users are allocated increased transmission power as compared to users operating under improved channel conditions [24]–[26]. Such an approach clearly improves the communication systems' overall fairness. It is noted that since users within one group share the available for the group communication resources, user grouping strategies can significantly influence the overall NOMA

Manuscript received October 20, 2017; revised January 8, 2018 and March 5, 2018; accepted March 22, 2018. Date of publication March 27, 2018; date of current version June 8, 2018. This work was support by the National Natural Science Foundation of China under Grant 61671072. *(Corresponding author: Tiejun Lv.)*

T. Lv, Y. Ma, and J. Zeng are with the School of Information and Communication Engineering, Beijing University of Posts and Telecommunications, Beijing 100876, China (e-mail: lvtiejun@bupt.edu.cn; mayy@bupt.edu.cn; zengjie@bupt.edu.cn).

P. T. Mathiopoulos is with the Department of Informatics and Telecommunications, National and Kapodistrian University of Athens, 157 84 Athens, Greece (e-mail: mathio@di.uoa.gr).

Digital Object Identifier 10.1109/JIOT.2018.2819645

2327-4662 © 2018 IEEE. Personal use is permitted, but republication/redistribution requires IEEE permission.
See http://www.ieee.org/publications_standards/publications/rights/index.html for more information.

system performance [27], and thus it is necessary to carefully study user scheduling schemes [28]–[31].

Due to the high demand of bandwidth required to support significantly increased data rates, the use of NOMA in conjunction with millimeter wave (mmWave) has become a natural choice for 5G systems [32]–[34]. For example, Zhang *et al.* [32] have proposed a cooperative mmWave-NOMA multicast scheme to improve the mmWave-NOMA multicasting. In [33], the performance of a NOMA cellular system operating at mmWave frequencies has been studied. By considering key features of mmWave systems, such as the high directionality of mmWave transmissions, the performance of the mmWave-NOMA system was analyzed in [34]. From these and other references it has become clear that through the use of mmWave-NOMA transmission the very demanding performance requirements of cellular M2M communications for IoT applications can be achieved.

Device-to-device (D2D) and M2M communications based on mmWave or NOMA technologies have also attracted considerable attention in both industrial and academic communities [9], [12], [13], [35], [36]. For example, Liu and Ansari [9] have proposed a novel architecture of green relay assisted D2D communications with dual battery for the IoT. The capability of mmWave communications for IoT-cloud supported autonomous vehicles was explored in [35]. A new multiple-input multiple-output NOMA scheme for small packet transmissions for IoT applications, based on the requirement that some devices need to be served quickly, was investigated in [36]. Shirvanimoghaddam *et al.* [13] presented an overview of 3GPP solutions for enabling massive cellular IoT and investigated random access strategies for M2M communications. Their research has shown that cellular networks should further evolve in order to support massive connectivity and low latency. In [15], NOMA was employed to support a large number of devices in cellular systems with limited radio resources. A mmWave-NOMA-based relaying scheme was proposed in [37] aiming at supporting IoT applications. Yang *et al.* [12], [38] have studied energy-efficient resource allocation for an M2M enabled cellular network. From all the above mentioned references, it is clear that the combination of M2M communications and cellular wireless communications is essential for the IoT. This combination, in conjunction with the massive connectivity requirements of the IoT, should lead to the use of appropriately modified multiple access techniques. Since in NOMA, a pair of devices share the same communication resources, device pairing can play a key role in improving the performance of NOMA systems. However, to the best of our knowledge, the idea of considering appropriate, MTC device pairing schemes, in conjunction with NOMA transmission for IoT applications, has not yet been studied in the open technical literature.

Motivated by the above, in this paper we propose a novel mmWave NOMA transmission system for cellular M2M communications tailored for IoT applications. For its efficient operation we effectively pair MTC devices, using three schemes, according to their distances from the base station (BS), as follows: 1) random near MTC device and another one randomly selected far MTC device (RNRF), i.e., one near MTC device and one far MTC device are randomly selected from two different groups; 2) the nearest near MTC device and the nearest far MTC device (NNNF), in which the nearest near MTC device and the nearest far MTC device are selected from two different groups; and 3) the nearest near MTC device and the farthest far MTC device (NNFF), in which the nearest near MTC device and the farthest far MTC device are selected from two different groups. The main advantages and novelties of the proposed mmWave NOMA scheme can be summarized as follows.

1) Due to the high directionality of mmWaves and the excellent collision avoidance of NOMA, the proposed mmWave-NOMA transmission system is capable of achieving massive connectivity in cellular M2M communications. Furthermore, it is shown that by employing random beamforming it is not required from all MTC devices to provide their channel state information (CSI) to the BS, which naturally leads to reduced overhead and latency.
2) Focusing on a single beam, we employ the above mentioned three MTC device pairing schemes which take MTC devices' locations into account, in conjunction with this mmWave-NOMA transmission scheme. These pairing schemes do not require that the BS has of their CSI, thereby reducing the system overhead. Moreover, transmissions of the MTC devices requiring different channel conditions are easily implemented in NOMA so that the QoS requirements of MTC devices can be easily achieved.
3) Closed-form expressions of the outage probability and sum rate at near MTC devices and far MTC devices are derived for all three MTC device pairing schemes operating in a cellular M2M communication environment and employing the proposed mmWave-NOMA transmission scheme. By analyzing their performance, it is theoretically proven that among the three pairing schemes, NNNF achieves the lowest outage probability both for near MTC and far MTC devices.

The rest of this paper is organized as follows. Section II presents the proposed mmWave-NOMA transmission scheme in cellular M2M communications. In Section III, the closed-form expressions of outage probability and sum rate for the proposed MTC device pairing schemes in cellular M2M communications for the IoT are derived. Section IV presents and discusses various performance evaluation results obtained my means of computer simulations as well as related discussion. Finally, the conclusions of the paper can be found in Section V.

II. System Model

In this section, we first present the channel model used in the considered communication system followed by the detailed description of the proposed transmission scheme. Then, a detailed derivation of the signal-to-interference-plus-noise ratio (SINR) for the MTC devices will be presented.

A. Channel Model

Following [34] and [39], a typical mmWave channel contains a line-of-sight (LOS) path and several nonline-of-sight

(NLOS) paths. Therefore, the mmWave channel vector from the BS to MTC device k can be mathematically modeled as

$$\mathbf{h}_k = \sqrt{M}\frac{\alpha_{k,L}\mathbf{a}\left(\theta_{k,L}\right)}{\sqrt{1+d_k^{\alpha_L}}} + \sqrt{M}\sum_{l=1}^{L}\frac{\alpha_{k,NL}\mathbf{a}\left(\theta_{k,NL}^{l}\right)}{\sqrt{1+d_k^{\alpha_{NL}}}} \tag{1}$$

where $\alpha_{k,L}$ and $\theta_{k,L}$ represent the complex gain and normalized direction of MTC device k for the LOS path, respectively; $\alpha_{k,NL}$ and $\theta_{k,NL}$ represent the complex gain and the normalized direction of MTC device k for the NLOS path, respectively; L is the number of NLOS paths, and α_L and α_{NL} are the path loss exponents for the LOS and the NLOS path, respectively; and d_k denotes the distance from the BS to MTC device k. In addition, $\mathbf{a}(\theta)$ is an array steering vector which can be expressed as

$$\mathbf{a}(\theta) = \frac{1}{\sqrt{M}}\left[1, e^{-j\pi\theta}, \ldots, e^{-j\pi(M-1)\theta}\right]^{\mathrm{T}} \tag{2}$$

where $[\,\cdot\,]^{\mathrm{T}}$ indicates the transpose of matrix.

In mmWave communication systems, the effect of LOS path is dominant because the path loss of NLOS exponents is much larger than that of the LOS exponent, e.g., the power of the signal following the LOS path is 20 dB higher than the power of the signals following the NLOS paths [39]. Consequently, the dominant path is the LOS path if such path exists, or the dominant path is one of the NLOS paths if an LOS path does not exist. Similar to [34] and [39], we adopt the single-path model, so that the considered mmWave channel simplifies to

$$\mathbf{h}_k = \sqrt{M}\frac{\alpha_k\mathbf{a}(\theta_k)}{\sqrt{1+d_k^{\alpha}}} \tag{3}$$

where α_k is the complex gain of MTC device k and follows the complex Gaussian distribution with zero mean and variance 1, i.e., $\alpha_k \sim \mathcal{CN}(0,1)$; θ_k is the normalized direction of the dominant path for MTC device k, and $\theta_k \sim \mathrm{Unif}[-1,1]$, i.e., θ_k is uniformly distributed between -1 and 1, while α is the path loss exponent.

B. mmWave-NOMA Transmission

Since conventional beamforming requires that all MTC devices provide their CSI to the BS, system overhead and latency are inevitably increased. In order to reduce them, random beamforming is employed, with each beam servicing two MTC devices. For simplicity, we focus on a single beam, which can be applied in a straight-forward way to the to multiple-beam case. The single beam generated by the BS can be expressed as

$$\mathbf{p} = \mathbf{a}(\nu) \tag{4}$$

Similar to [34] and [39], in (4) ν is a random variable with uniformly distributed between -1 and 1, i.e., $\nu \sim \mathrm{Unif}[-1,1]$. Note that $\mathbf{a}(\nu)$ is given by (2).

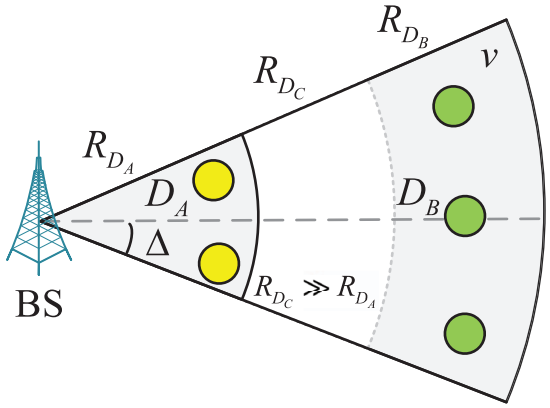

Fig. 1. Proposed mmWave-NOMA downlink transmission scheme in cellular M2M communications for IoT, which include a BS and two groups of MTC devices, $A = \{A_i\}$ and $B = \{B_j\}$ located in the regions D_A and D_B, respectively, which have a central angle of 2Δ. Distributions of the near MTC device (yellow circles) and the far MTC device (green circles) follow HPPPs. The MTC devices located in D_A and D_B will be scheduled.

According to [34] and [39], the effective channel gain of the MTC device k, $|\mathbf{h}_k^H\mathbf{p}|^2$, can be expressed as

$$\begin{aligned}\left|\mathbf{h}_k^H\mathbf{p}\right|^2 &= \frac{M|\alpha_k|^2\left|\mathbf{a}(\theta_k)^H\mathbf{p}\right|^2}{1+d_k^{\alpha}} \\ &= \frac{|\alpha_k|^2\left|\sum_{n=0}^{M-1} e^{-j\pi n(\nu-\theta_k)}\right|^2}{M\left(1+d_k^{\alpha}\right)} \\ &= \frac{|\alpha_k|^2\sin^2\left(\frac{\pi M(\nu-\theta_k)}{2}\right)}{M\left(1+d_k^{\alpha}\right)\sin^2\left(\frac{\pi(\nu-\theta_k)}{2}\right)} \\ &= \frac{|\alpha_k|^2}{\left(1+d_k^{\alpha}\right)}F_M(\nu-\theta_k)\end{aligned} \tag{5}$$

where $F_M(\cdot)$ is the *Fejér kernel*. By increasing $(\nu-\theta_k)$, $F_M(\nu-\theta_k)$ goes to zero quickly. If the direction of channel vector of MTC device k aligns with the direction of the beam $\mathbf{p}$, the MTC device will have a large effective channel gain. Furthermore, having a large number of MTC devices increases the probability of alignment so that massive connectivity can be more effectively supported by using a mmWave-NOMA transmission scheme.

In this paper, we introduce a new mmWave-NOMA downlink transmission scheme designed for cellular M2M communications for IoT applications for which one BS serves two groups of MTC devices $A = \{A_i\}$ and $B = \{B_j\}$, where $i = 1, 2, \ldots, N_A$ and $j = 1, 2, \ldots, N_B$. $N_k (k \in \{A, B\})$ denotes the number of MTC devices in two groups. The BS is equipped with M transmit antennas and is located at the center of the cell while each MTC device is equipped with a single antenna. As illustrated in Fig. 1, and according to the operation of the proposed transmission scheme, MTC devices are located at the wedge-shaped sector D_A, with an angle of 2Δ and a radius R_{D_A}, and at the sector ring D_B with a maximum radius R_{D_B} and a minimum radius R_{D_C}, are scheduled. It is noted that for the limiting case of $\Delta \to 0$, a large effective channel gain can be achieved.

We consider the scenario where the MTC devices in group A are deployed within the wedge-shaped sector D_A, and the devices in group B are deployed within the sector ring D_B. It is also assumed that $R_{D_C} \gg R_{D_A}$ so that the channel conditions in these two coverage areas are different for the two groups of MTC devices [40]. It is further assumed that the MTC devices are randomly deployed within the wedge-shaped sector D_A and the sector ring D_B, and that they follow a homogeneous Poisson point process $\Phi_k (k \in \{A, B\})$ with density λ_k. Thus, the probability distribution of $N_k (k \in \{A, B\})$ is $P(N_k = n) = \mu_k^n e^{-\mu_k}/n!$, where $\mu_A = \Delta R_{D_A}^2 \lambda_A$ and $\mu_B = \Delta (R_{D_B}^2 - R_{D_C}^2)\lambda_B$.

As previously mentioned, two MTC devices are selected to implement NOMA, with one of them belonging to group A and the other one to group B. Furthermore, based on the locations of MTC devices, we consider the following three MTC device pairing schemes to perform NOMA: 1) RNRF are randomly selected from the two groups; 2) NNNF are selected from the two groups; and 3) NNFF are selected from the two groups.

C. SINR of MTC Devices

Let us select one MTC device from each of the two MTC device groups, and the two selected MTC devices are paired to perform NOMA, so that $N_k \geq 1 (k \in \{A, B\})$. The BS broadcasts the signal $\mathbf{p}(\beta_{i1} s_{A_i} + \beta_{i2} s_{B_i})$ to the near MTC device A_i and the far MTC device B_i, where s_{A_i} and s_{B_i} are the transmit signals of A_i and B_i, and β_{i1} and β_{i2} are their power allocations, respectively, with $\beta_{i1} < \beta_{i2}$, and $\beta_{i1}^2 + \beta_{i2}^2 = 1$.

The received signal at the MTC device A_i is expressed as

$$y_{A_i} = \mathbf{h}_{A_i}^H \mathbf{p}\big(\beta_{i1} s_{A_i} + \beta_{i2} s_{B_i}\big) + n_{A_i} \tag{6}$$

where n_{A_i} represents additive white complex Gaussian noise.

Considering SIC at the receiver, the MTC device A_i first decodes the signal of B_i, so that the SINR of B_i at the receiver of A_i can be expressed as

$$\mathrm{SINR}_{B_i \to A_i} = \frac{\rho \left| \mathbf{h}_{A_i}^H \mathbf{p} \right|^2 \beta_{i2}^2}{\rho \left| \mathbf{h}_{A_i}^H \mathbf{p} \right|^2 \beta_{i1}^2 + 1} \tag{7}$$

where ρ denotes the transmit signal-to-noise ratio (SNR). Then, A_i decodes its own signal, so the SNR of A_i is expressed as

$$\mathrm{SINR}_{A_i} = \rho \left| \mathbf{h}_{A_i}^H \mathbf{p} \right|^2 \beta_{i1}^2. \tag{8}$$

Similarly, since the MTC device B_i decodes its own signal by treating the signal of MTC device A_i as noise, the SINR of B_i is expressed as

$$\mathrm{SINR}_{B_i} = \frac{\rho \left| \mathbf{h}_{B_i}^H \mathbf{p} \right|^2 \beta_{i2}^2}{\rho \left| \mathbf{h}_{B_i}^H \mathbf{p} \right|^2 \beta_{i1}^2 + 1}. \tag{9}$$

III. Performance Analysis of the MTC Device Pairing Schemes

To guarantee the QoS required by the MTC devices, we define R_1 and R_2 as the minimum sum rate of the near MTC device and the far MTC device, respectively, and that $\epsilon_{A_i} = 2^{R_1} - 1$ and $\epsilon_{B_i} = 2^{R_2} - 1$. When the near MTC device A_i cannot decode successfully the signal of the far MTC device B_i nor its own signal, outage of the MTC device A_i occurs with the following probability:

$$P_{A_i}^o = 1 - P\big(\mathrm{SINR}_{B_i \to A_i} > \epsilon_{B_i}, \mathrm{SINR}_{A_i} > \epsilon_{A_i}\big). \tag{10}$$

Furthermore, the outage probability of MTC device B_i is formulated as

$$P_{B_i}^o = P\big(\mathrm{SINR}_{B_i} < \epsilon_{B_i}\big). \tag{11}$$

Using (10) and (11), the outage sum rate of cellular M2M communications with the mmWave-NOMA transmission scheme can be expressed as

$$R_{\mathrm{NOMA}} = \big(1 - P_{A_i}^o\big) R_{A_i} + \big(1 - P_{B_i}^o\big) R_{B_i} \tag{12}$$

while the equivalent outage sum rate of cellular M2M communications with the mmWave-OMA transmission scheme can be expressed as

$$R_{\mathrm{OMA}} = \big(1 - P_{A_i}\big) R_{A_i}^O + \big(1 - P_{B_i}\big) R_{B_i}^O \tag{13}$$

where

$$P_n = P\Big(\log\Big(1 + \rho \left| \mathbf{h}_n^H \mathbf{p} \right|^2\Big) < 2R_n^O\Big), n \in \{A_i, B_i\}$$

and

$$R_n^O = \frac{1}{2} \log\Big(1 + \rho \left| \mathbf{h}_n^H \mathbf{p} \right|^2\Big), n \in \{A_i, B_i\}. \tag{14}$$

The reason why the term 1/2 appears in (14) is the fact that the two MTC devices use a resource block, which is shared by two MTC devices in NOMA transmissions [27], [28].

Next, we will analyze the performance of the three MTC device pairing schemes.

A. RNRF Pairing Scheme

For this scheme, a near MTC device A_i and a far MTC device B_i are randomly selected from the two groups with equal probability to be served with the NOMA protocol. It is noted that, since the BS does not require any CSI based on random selection of the MTC devices, the system overhead is significantly reduced.

1) Outage Probability of the MTC Near Device of RNRF: In principle, the outage probability can be obtained by evaluating (10) using (5), (7), and (8). However, it is not difficult to realize that this is a very complex task as its solution involves a nondeterministic polynomial-time hard problem. Instead, we will consider the limiting cases for $\Delta \to 0$ and high SNR to obtain the outage probability performance. For this, the following theorem will be used to obtain the outage probability of the near MTC device of RNRF for arbitrary values of path loss exponent, α.

Theorem 1: For $\Delta \to 0$ and high SNR, the outage probability of the near MTC device A_i of RNRF can be approximated as

$$P_{A_i}^o \approx \frac{\eta_{A_i}}{M} \left(2 + \frac{\pi^2 M^2 \Delta^2}{18}\right) \left(\frac{1}{2} + \frac{R_{D_A}^\alpha}{\alpha + 2}\right) \tag{15}$$

if $\beta_{i2}^2 - \beta_{i1}^2\epsilon_{B_i} > 0$; otherwise $P_{A_i}^o = 1$. In the above equation, $\eta_{A_i} = \max\{(\epsilon_{B_i}/[\rho(\beta_{i2}^2 - \beta_{i1}^2\epsilon_{B_i})]), (\epsilon_{A_i}/\rho\beta_{i1}^2)\}$.

Proof: $\beta_{i2}^2 - \beta_{i1}^2\epsilon_{B_i} \leq 0$ indicates that the near MTC device cannot decode the signal of the far MTC device successfully, hence $P_{A_i}^o = 1$. When $\beta_{i2}^2 - \beta_{i1}^2\epsilon_{B_i} > 0$, (15) will be derived as follows.

The MTC devices are deployed in D_A following homogeneous Poisson point processes (HPPPs), so they are independently and identically distributed (i.i.d) points, denoted by W_{A_i}, considering the location information A_i. Therefore, the probability density function (PDF) of W_{A_i} can be expressed as

$$f_{W_{A_i}}(w_{A_i}) = \frac{\lambda_A}{\mu_A} = \frac{1}{\Delta R_{D_A}^2}. \tag{16}$$

Then, the outage probability of the near MTC device A_i is given by

$$\begin{aligned} P_{A_i}^o &= \int_{D_A}\left(1 - e^{-\frac{\eta_{A_i}\left(1+d_{A_i}^{\alpha}\right)}{F_M\left(\nu-\theta_{A_i}\right)}}\right) f_{W_{A_i}}(w_{A_i})dw_{A_i} \\ &= \frac{1}{\Delta R_{D_A}^2}\int_{\nu-\Delta}^{\nu+\Delta}\int_0^{R_{D_A}}(1 - e^{-\frac{\eta_{A_i}(1+r^{\alpha})}{F_M(\nu-\theta)}})rdrd\theta \end{aligned} \tag{17}$$

where $\eta_{A_i} = \max\{(\epsilon_{B_i}/[\rho(\beta_{i2}^2 - \beta_{i1}^2\epsilon_{B_i})]), (\epsilon_{A_i}/\rho\beta_{i1}^2)\}$. According to (5), the *Fejér kernel* can be written as

$$F_M(\nu-\theta) = \frac{\sin^2\left(\frac{\pi M(\nu-\theta)}{2}\right)}{M\sin^2\left(\frac{\pi(\nu-\theta)}{2}\right)}. \tag{18}$$

Noting that $|\nu - \theta| \leq \Delta$, and following [34], for $\Delta \to 0$, the *Fejér kernel* can be approximated as

$$\begin{aligned} F_M(\nu-\theta) &\approx M\text{sinc}^2\left(\frac{\pi M(\nu-\theta)}{2}\right) \\ &\approx M\left(1 - \frac{\pi^2M^2(\nu-\theta)^2}{12}\right). \end{aligned} \tag{19}$$

In deriving (19) the following approximations have been used: $\sin(x) \approx x$ for $x \to 0$, $\text{sinc}(x) \approx (1-[x^2/6])$ and $(1-x)^2 \approx 2x$ for $x \to 0$.

Therefore, (17) can be approximated as

$$\begin{aligned} P_{A_i}^o &\approx \int_{\nu-\Delta}^{\nu+\Delta}\int_0^{R_{D_A}}\frac{1}{\Delta R_{D_A}^2}\times\left(1 - e^{-\frac{\eta_{A_i}(1+r^{\alpha})}{M\left(1-\frac{\pi^2M^2(\nu-\theta)^2}{12}\right)}}\right)rdrd\theta \\ &\approx \int_{\nu-\Delta}^{\nu+\Delta}\int_0^{R_{D_A}}\frac{1}{\Delta R_{D_A}^2} \\ &\quad\times\left(1 - e^{-\frac{\eta_{A_i}(1+r^{\alpha})}{M}\left(1+\frac{\pi^2M^2(\nu-\theta)^2}{12}\right)}\right)rdrd\theta \end{aligned} \tag{20}$$

where the second approximation holds because of $(1-x)^{-1} \approx (1+x)$ for $x \to 0$.

Additionally, since η_{A_i} goes to zero at high SNR, $(1-e^{-x}) \approx x$ for $x \to 0$ can be used to approximate (20) as

$$\begin{aligned} P_{A_i}^o &\approx \frac{1}{\Delta R_{D_A}^2}\int_{\nu-\Delta}^{\nu+\Delta}\int_0^{R_{D_A}}\frac{\eta_{A_i}(1+r^{\alpha})}{M} \\ &\quad\times\left(1 + \frac{\pi^2M^2(\nu-\theta)^2}{12}\right)rdrd\theta. \end{aligned} \tag{21}$$

From (21) and after some straightforward mathematical manipulations, (15) can be easily derived. ■

2) Outage Probability of the Far MTC Device of RNRF: According to the NOMA principle, the outage of the far MTC device B_i appears when it cannot decode its own signal successfully. Again considering the limiting cases for $\Delta \to 0$ and high SNR, the following theorem gives the outage probability of the far MTC device of RNRF for arbitrary values of path loss exponent, α.

Theorem 2: For $\Delta \to 0$ and high SNR, the outage probability of the far MTC device B_i of RNRF can be approximated as

$$\begin{aligned} P_{B_i}^o &\approx \frac{\eta_{B_i}}{M\left(R_{D_B}^2 - R_{D_C}^2\right)}\left(2 + \frac{\pi^2M^2\Delta^2}{18}\right) \\ &\quad\times\left(\frac{R_{D_B}^2 - R_{D_C}^2}{2} + \frac{R_{D_B}^{\alpha+2} - R_{D_C}^{\alpha+2}}{\alpha+2}\right) \end{aligned} \tag{22}$$

if $\beta_{i2}^2 - \beta_{i1}^2\epsilon_{B_i} > 0$; otherwise $P_{B_i}^o = 1$. In (22), $\eta_{B_i} = (\epsilon_{B_i}/[\rho(\beta_{i2}^2 - \beta_{i1}^2\epsilon_{B_i})])$.

Proof: Similar to the near MTC device case, the far MTC device cannot decode its own signal successfully when $\beta_{i2}^2 - \beta_{i1}^2\epsilon_{B_i} \leq 0$, i.e., $P_{B_i}^o = 1$. Next, the outage probability of the far MTC device will be derived when $\beta_{i2}^2 - \beta_{i1}^2\epsilon_{B_i} > 0$.

Similar to the near MTC device A_i case, the PDF of W_{B_i} can be expressed as

$$f_{W_{B_i}}(w_{B_i}) = \frac{\lambda_B}{\mu_B} = \frac{1}{\Delta\left(R_{D_B}^2 - R_{D_C}^2\right)}. \tag{23}$$

Therefore, the outage probability of the far MTC device B_i is given by

$$\begin{aligned} P_{B_i}^o &= \int_{D_B}\left(1 - e^{-\frac{\eta_{B_i}\left(1+d_{B_i}^{\alpha}\right)}{F_M\left(\nu-\theta_{B_i}\right)}}\right)f_{W_{B_i}}(w_{B_i})dw_{B_i} \\ &= \frac{1}{\Delta\left(R_{D_B}^2 - R_{D_C}^2\right)}\int_{\nu-\Delta}^{\nu+\Delta}\int_{R_{D_C}}^{R_{D_B}}\left(1 - e^{-\frac{\eta_{B_i}(1+r^{\alpha})}{F_M(\nu-\theta)}}\right)rdrd\theta \end{aligned} \tag{24}$$

where $\eta_{B_i} = (\epsilon_{B_i}/[\rho(\beta_{i2}^2 - \beta_{i1}^2\epsilon_{B_i})])$.

Following a similar procedure as for the near MTC device case, the approximation of (24) can be obtained as

$$\begin{aligned} P_{B_i}^o &\approx \frac{1}{\Delta(R_{D_B}^2 - R_{D_C}^2)}\int_{\nu-\Delta}^{\nu+\Delta}\int_{R_{D_C}}^{R_{D_B}}\frac{\eta_{B_i}(1+r^{\alpha})}{M} \\ &\quad\times\left(1 + \frac{\pi^2M^2(\nu-\theta)^2}{12}\right)rdrd\theta. \end{aligned} \tag{25}$$

From (25) and after some straightforward mathematical manipulations, (22) can be easily derived. ■

B. NNNF Pairing Scheme

For this scheme, we select an MTC device within the wedge-shaped sector D_A which has the shortest distance to the BS as the near MTC device A_{i^*}. Similarly, we select an MTC device within the sector ring D_B which has the shortest distance to the BS as the far MTC device B_{i^*}. Because of these choices, this scheme can achieve the minimum outage probability of both the near and far MTC devices, which can be considered as an upper bound on the performance. In this case, the BS needs to know only the MTC devices' distance information in NNNF, which leads to a lower system overhead as compared to requiring the knowledge of the MTC devices' effective channel gains.

1) Outage Probability of the Near MTC Device of NNNF: Similar to the case of RNRF, the outage of the near MTC device A_{i^*} can occur for two reasons. The first one is that the near MTC device A_{i^*} cannot decode the signal of the far MTC device B_{i^*} successfully, while the second one is that the near MTC device A_{i^*} cannot decode its own signal successfully. Based on these, we can analytically obtain the outage probability of the near MTC device of NNNF. The following theorem gives the outage probability of the near MTC device of NNNF for an arbitrary choice of path loss exponent, α.

Theorem 3: For $\Delta \to 0$ and high SNR, the outage probability of the near MTC device A_{i^*} of NNNF can be approximated as (26), shown at the bottom of the next page, if $\beta_{i2}^2 - \beta_{i1}^2 \epsilon_{B_i} > 0$; otherwise $P_{A_{i^*}}^o = 1$. In (26), $\gamma(\cdot)$ denotes the incomplete gamma function.

Proof: The near MTC device cannot decode the signal of the far MTC device successfully when $\beta_{i2}^2 - \beta_{i1}^2 \epsilon_{B_i} \leq 0$, i.e., $P_{A_{i^*}}^o = 1$. Next, the outage probability of the near MTC device will be considered when $\beta_{i2}^2 - \beta_{i1}^2 \epsilon_{B_i} > 0$.

The distance between the nearest A_{i^*} and the BS is denoted by $d_{A_{i^*}}$. The probability $\Pr(d_{A_{i^*}} > r \mid N_A \geq 1)$ conditioned on $N_A \geq 1$ implies that there is no device located in the sector with radius r, which is expressed as

$$\Pr\left(d_{A_{i^*}} > r \mid N_A \geq 1\right) = \frac{\Pr\left(d_{A_{i^*}} > r\right) - \Pr\left(d_{A_{i^*}} > r, N_A = 0\right)}{\Pr(N_A \geq 1)} = \frac{e^{-\Delta\lambda_A r^2} - e^{-\Delta\lambda_A R_{D_A}^2}}{1 - e^{-\Delta\lambda_A R_{D_A}^2}}. \quad (27)$$

According to the above expression, the location information about A_{i^*} can be obtained. Therefore, the PDF of $d_{A_{i^*}}$ is given by

$$f_{d_{A_{i^*}}(r_A)} = \frac{2\Delta\lambda_A r_A}{1 - e^{-\Delta\lambda_A R_{D_A}^2}} e^{-\Delta\lambda_A r_A^2}. \quad (28)$$

Next, the outage probability of the nearest near MTC device A_{i^*} is given by

$$P_{A_{i^*}}^o = \int_{\nu-\Delta}^{\nu+\Delta} \int_0^{R_{D_A}} \left(1 - e^{-\frac{\eta_{A_i}(1+r^\alpha)}{F_M(\nu-\theta)}}\right) \frac{f_{d_{A_{i^*}}(r)}}{2\Delta} dr d\theta. \quad (29)$$

Similar to the near MTC device A_i of RNRF, (29) can be approximated as

$$P_{A_{i^*}}^o \approx \int_{\nu-\Delta}^{\nu+\Delta} \int_0^{R_{D_A}} \frac{\eta_{A_i}(1+r^\alpha)}{M} \times \left(1 + \frac{\pi^2 M^2 (\nu-\theta)^2}{12}\right) \frac{f_{d_{A_{i^*}}(r)}}{2\Delta} dr d\theta. \quad (30)$$

From (30) and after some straightforward mathematical manipulations, (26) can be easily derived. ■

2) Outage Probability of the Far MTC Device of NNNF: Similar to the far MTC device of RNRF, the outage of the far MTC device B_{i^*} occurs for one situation, namely when the far MTC device B_{i^*} cannot decode its own signal successfully. This case characterizes the occurrence of the outage probability for the far MTC which can be obtained for an arbitrary choice of path loss exponent, α, through the following theorem.

Theorem 4: For $\Delta \to 0$ and high SNR, the outage probability of the far MTC device B_{i^*} of NNNF can be approximated as (31), shown at the bottom of the next page, if $\beta_{i2}^2 - \beta_{i1}^2 \epsilon_{B_i} > 0$; otherwise $P_{B_{i^*}}^o = 1$.

Proof: The far MTC device cannot decode its own signal successfully when $\beta_{i2}^2 - \beta_{i1}^2 \epsilon_{B_i} \leq 0$, i.e., $P_{B_{i^*}}^o = 1$. When $\beta_{i2}^2 - \beta_{i1}^2 \epsilon_{B_i} > 0$ the outage probability of the far MTC device will be obtained next.

The distance between the nearest B_{i^*} and the BS is denoted by $d_{B_{i^*}}$. Similar to (28), the PDF of $d_{B_{i^*}}$ is expressed as

$$f_{d_{B_{i^*}}(r_B)} = \frac{2\Delta\lambda_B r_B}{1 - e^{-\Delta\lambda_B\left(R_{D_B}^2 - R_{D_C}^2\right)}} e^{-\Delta\lambda_B\left(r_B^2 - R_{D_C}^2\right)}. \quad (32)$$

Then, the outage probability of the nearest far MTC device B_{i^*} is given by

$$P_{B_{i^*}}^o = \int_{\nu-\Delta}^{\nu+\Delta} \int_{R_{D_C}}^{R_{D_B}} \left(1 - e^{-\frac{\eta_{B_i}(1+r^\alpha)}{F_M(\nu-\theta)}}\right) \frac{f_{d_{B_{i^*}}(r)}}{2\Delta} dr d\theta. \quad (33)$$

Similar to (21) and (33) can be approximated as

$$P_{B_{i^*}}^o \approx \int_{\nu-\Delta}^{\nu+\Delta} \int_{R_{D_C}}^{R_{D_B}} \frac{\eta_{B_i}(1+r^\alpha)}{M} \times \left(1 + \frac{\pi^2 M^2 (\nu-\theta)^2}{12}\right) \frac{f_{d_{B_{i^*}}(r)}}{2\Delta} dr d\theta. \quad (34)$$

From (34) and after some straightforward mathematical manipulations, (31) can be easily derived. ■

C. NNFF Pairing Scheme

For this scheme, we select, within the sector D_A, an MTC device which has the shortest distance to the BS as the near MTC device $A_{i'}$. Similarly, we select an MTC device within the sector ring D_B which has the farthest distance to the BS as the far MTC device $B_{i'}$. If MTC device channel conditions are bigger differences, NOMA can achieve a larger performance gain over OMA, which leads to the NNFF MTC device pairing scheme.

1) Outage Probability of the Near MTC Device of NNFF: Similarly to the NNNF case, here also the near MTC device is selected in the same way. In addition, their power allocation factors are identical. Therefore, outage probability of the near MTC device $A_{i'}$ is the same as the outage probability of A_{i^*} of NNNF. The approximation of its outage probability expression is given by (26), and the proof is the same as that of the Theorem 3.

2) Outage Probability of the Far MTC Device of NNFF: Similar to the far MTC device of RNRF, the outage of the far MTC device $B_{i'}$ occurs only when the far MTC device $B_{i'}$ cannot decode its own signal successfully. Based on the outage of the far MTC device of NNFF, its outage probability can be obtained for arbitrarily values of α, using the following theorem.

Theorem 5: For $\Delta \to 0$ and high SNR, the outage probability of the far MTC device $B_{i'}$ of NNFF can be approximated as

$$P^o_{B_{i'}} \approx \frac{\eta_{B_i}\lambda_B}{M\left(1-e^{-\Delta\lambda_B\left(R^2_{D_B}-R^2_{D_C}\right)}\right)}\left(2\Delta+\frac{\pi^2M^2\Delta^3}{18}\right) \times e^{-\Delta\lambda_B R^2_{D_B}}\left(\frac{e^{\Delta\lambda_B R^2_{D_B}}-e^{\Delta\lambda_B R^2_{D_C}}}{2\Delta\lambda_B}+\Omega\right) \quad (35)$$

if $\beta^2_{i2}-\beta^2_{i1}\epsilon_{B_i} > 0$; otherwise $P^o_{B_{i'}} = 1$. In (35), $\Omega = \int_{R_{D_C}}^{R_{D_B}} r^{\alpha+1}e^{\Delta\lambda_B r^2}dr$.

Proof: The far MTC device cannot decode its own signal successfully when $\beta^2_{i2}-\beta^2_{i1}\epsilon_{B_i} \le 0$, i.e., $P^o_{B_{i'}} = 1$. When $\beta^2_{i2}-\beta^2_{i1}\epsilon_{B_i} > 0$, the outage probability of the far MTC device can be obtained as follows.

Let us denote the distance between the farthest $B_{i'}$ and the BS as $d_{B_{i'}}$, and the number of MTC devices in D_B as N_B. Similar to (28), the PDF of $d_{B_{i'}}$ can be expressed as

$$f_{d_{B_{i'}}(r_B)} = \frac{2\Delta\lambda_B r_B}{1-e^{-\Delta\lambda_B\left(R^2_{D_B}-R^2_{D_C}\right)}}e^{-\Delta\lambda_B\left(R^2_{D_B}-r^2_B\right)}. \quad (36)$$

Then, the outage probability of the farthest far MTC device $B_{i'}$ is given by

$$P^o_{B_{i'}} = \int_{\nu-\Delta}^{\nu+\Delta}\int_{R_{D_C}}^{R_{D_B}}\left(1-e^{-\frac{\eta_{B_i}(1+r^\alpha)}{FM(\nu-\theta)}}\right)\frac{f_{d_{B_{i'}}(r)}}{2\Delta}drd\theta. \quad (37)$$

Similar to (22) and (37) can be approximated as

$$P^o_{B_{i'}} \approx \int_{\nu-\Delta}^{\nu+\Delta}\int_{R_{D_C}}^{R_{D_B}}\frac{\eta_{B_i}(1+r^\alpha)}{M} \times\left(1+\frac{\pi^2M^2(\nu-\theta)^2}{12}\right)\frac{f_{d_{B_{i'}}(r)}}{2\Delta}drd\theta. \quad (38)$$

From (38) and after some straightforward mathematical manipulations, (35) can be easily derived. ■

Note that when α is a certain value, Ω has a closed-form expression.

Remark 1: For the design of practical IoT systems, if each MTC device requires the same opportunity served and the lowest latency transmission, RNRF should be considered first; if each MTC device requires the best possible performance and low-latency transmission, NNNF should be employed. As far as the NNFF scheme is concerned, large performance gain can be achieved if MTC device channel conditions are greatly different.

D. Performance Comparison of the Three Pairing Schemes

1) Near MTC Device: In order to compare its performance with that given by (15), (26) can be rewritten as

$$P^o_{A_{i^*}} \approx \frac{\eta_{A_i}}{M}\left(2+\frac{\pi^2M^2\Delta^2}{18}\right)\left(\frac{1}{2}+L_{A^*}\right) \quad (39)$$

where $L_{A^*} = (\Upsilon_{A^*}/[2(\Delta\lambda_A)^{(\alpha/2)}(1-e^{-\Delta\lambda_A R^2_{D_A}})])$, and $\Upsilon_{A^*} = \gamma((\alpha/2)+1, \Delta\lambda_A R^2_{D_A})$ is the incomplete gamma function. When $\Delta \to 0$, Υ_{A^*} can be approximated as

$$\Upsilon_{A^*} \approx \frac{2(\Delta\lambda_A)^{\frac{\alpha+2}{2}}R^{\alpha+2}_{D_A}}{\alpha+2} - \frac{2(\Delta\lambda_A)^{\frac{\alpha+4}{2}}R^{\alpha+4}_{D_A}}{\alpha+4} \quad (40)$$

as $(1-e^{-x}) \approx x$ (for $x \to 0$), and $(1-e^{-\Delta\lambda_A R^2_{D_A}}) \approx \Delta\lambda_A R^2_{D_A}$. Thus, L_{A^*} can be approximated as

$$L_{A^*} \approx \frac{R^\alpha_{D_A}}{\alpha+2} - \frac{\Delta\lambda_A R^{\alpha+2}_{D_A}}{\alpha+4}. \quad (41)$$

Obviously, we have $(R^\alpha_{D_A}/\alpha+2) < L_{A^*}$, which indicates the outage probabilities of the near MTC devices in NNNF and NNFF are lower than those of the near MTC devices in RNRF, i.e., $P^o_{A_i} > P^o_{A_{i^*}} = P^o_{A_{i'}}$.

$$P^o_{A_{i^*}} \approx \frac{\eta_{A_i}\lambda_A}{M\left(1-e^{-\Delta\lambda_A R^2_{D_A}}\right)}\left(2\Delta+\frac{\pi^2M^2\Delta^3}{18}\right)\left(\frac{1-e^{-\Delta\lambda_A R^2_{D_A}}}{2\Delta\lambda_A}+\frac{(\Delta\lambda_A)^{-\frac{\alpha+2}{2}}}{2}\gamma\left(\frac{\alpha}{2}+1, \Delta\lambda_A R^2_{D_A}\right)\right) \quad (26)$$

$$P^o_{B_{i^*}} \approx \frac{\eta_{B_i}\lambda_B}{M\left(1-e^{-\Delta\lambda_B\left(R^2_{D_B}-R^2_{D_C}\right)}\right)}\left(2\Delta+\frac{\pi^2M^2\Delta^3}{18}\right)e^{\Delta\lambda_B R^2_{D_C}} \times\left(\frac{e^{-\Delta\lambda_B R^2_{D_C}}-e^{-\Delta\lambda_B R^2_{D_B}}}{2\Delta\lambda_B}+\frac{(\Delta\lambda_B)^{-\frac{\alpha+2}{2}}}{2}\left(\gamma\left(\frac{\alpha}{2}+1, \Delta\lambda_B R^2_{D_B}\right)-\gamma\left(\frac{\alpha}{2}+1, \Delta\lambda_B R^2_{D_C}\right)\right)\right) \quad (31)$$

Consequently, it is clear that the performance of the near MTC devices' outage probability in NNNF equals that of NNFF, and the performance of the near MTC devices' outage probability in RNRF is the worst among the three proposed schemes.

2) Far MTC Device: Similar to the near MTC device, (31) can be approximated as

$$P^{o}_{B^*} \approx \frac{\eta_{B_i}}{M\left(R^2_{D_B} - R^2_{D_C}\right)}\left(2 + \frac{\pi^2 M^2 \Delta^2}{18}\right) L_{B^*} \tag{42}$$

where

$$L_{B^*} = e^{\Delta\lambda_B R^2_{D_C}}\left(\frac{e^{-\Delta\lambda_B R^2_{D_C}} - e^{-\Delta\lambda_B R^2_{D_B}}}{2\Delta\lambda_B} + \frac{(\Delta\lambda_B)^{-\frac{\alpha+2}{2}}}{2} \times \left(\gamma\left(\frac{\alpha}{2}+1, \Delta\lambda_B R^2_{D_B}\right) - \gamma\left(\frac{\alpha}{2}+1, \Delta\lambda_B R^2_{D_C}\right)\right)\right). \tag{43}$$

When $\Delta \to 0$, (43) can be approximated as

$$L_{B^*} \approx \frac{R^2_{D_B} - R^2_{D_C}}{2} + \frac{R^{\alpha+2}_{D_B} - R^{\alpha+2}_{D_C}}{\alpha+2} - \Delta\lambda_B \frac{R^{\alpha+4}_{D_B} - R^{\alpha+4}_{D_C}}{\alpha+4}. \tag{44}$$

Clearly, $([R^2_{D_B} - R^2_{D_C}]/2) + ([R^{\alpha+2}_{D_B} - R^{\alpha+2}_{D_C})]/[\alpha+2]) > L_{B^*}$, which indicates that the outage probability of the far MTC devices in NNNF is lower than that of the far MTC devices in RNRF, i.e., $P^{o}_{B_i} > P^{o}_{B_{i^*}}$.

Similar to the far MTC device in NNNF, (35) can be approximated as

$$P^{o}_{B'} \approx \frac{\eta_{B_i}}{M\left(R^2_{D_B} - R^2_{D_C}\right)}\left(2 + \frac{\pi^2 M^2 \Delta^2}{18}\right) L_{B'} \tag{45}$$

where

$$L_{B'} = e^{-\Delta\lambda_B R^2_{D_B}}\left(\frac{e^{\Delta\lambda_B R^2_{D_B}} - e^{\Delta\lambda_B R^2_{D_C}}}{2\Delta\lambda_B} + \Omega\right). \tag{46}$$

When $\Delta \to 0$, $L_{B'}$ can be approximated as

$$L_{B'} \approx \frac{R^2_{D_B} - R^2_{D_C}}{2} + \frac{R^{\alpha+2}_{D_B} - R^{\alpha+2}_{D_C}}{\alpha+2} + \Delta\lambda_B \frac{R^{\alpha+4}_{D_B} - R^{\alpha+4}_{D_C}}{\alpha+4}. \tag{47}$$

In this case, $([R^2_{D_B} - R^2_{D_C}]/2) + ([R^{\alpha+2}_{D_B} - R^{\alpha+2}_{D_C})]/[\alpha+2]) < L_{B'}$, which indicates that the outage probability of the far MTC devices in NNFF is worse than that of the far MTC devices in RNRF, i.e., $P^{o}_{B_i} < P^{o}_{B_{i'}}$.

In summary, among the three proposed MTC device pairing schemes, the performance of the far MTC devices' outage probability in NNNF is best, and the performance of the far MTC devices' outage probability in NNFF is worst, i.e., $P^{o}_{B_{i^*}} < P^{o}_{B_i} < P^{o}_{B_{i'}}$.

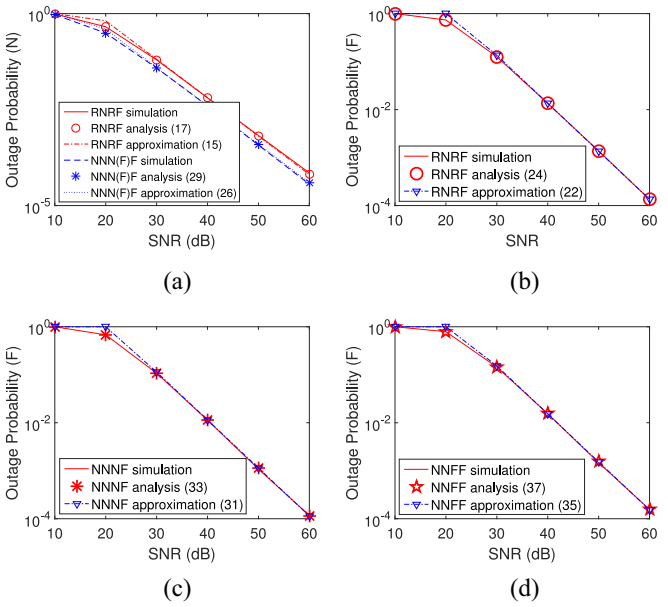

Fig. 2. Outage probability of MTC devices versus SNR. (a) Near MTC device in the three MTC device pairing schemes. Far MTC device in (b) RNRF, (c) NNNF, and (d) NNFF.

IV. Performances Evaluation Results and Discussion

In this section, various performance evaluation results for the operation of the three proposed MTC device pairing schemes obtained by means of computer simulations complementing the previously derived theoretical approach will be presented. Unless otherwise stated, the results have been obtained for the following system parameter values. The radius of the wedge-shaped sector D_A is set as $R_{D_A} = 2.5$ m, $\lambda_A = 6$, and $\Delta = 0.1$. The radius of the sector ring D_B is set as $R_{D_C} = 8$ m and $R_{D_B} = 10$ m, $\lambda_B = 2$. The number of transmit antennas of the BS is $M = 4$, and the path loss exponent is set as $\alpha = 2$. $\beta^2_{i1} = 0.25$ and $\beta^2_{i2} = 0.75$ are the power allocations for the near MTC device and the far MTC device, respectively, [34], [40]. The other parameters are set as $R_1 = 4$ bits per channel use (BPCU) and $R_2 = 1.5$ BPCU. In addition, we focus on LOS path in this paper.

Fig. 2 illustrates the outage probability versus SNR and includes Monte Carlo simulation results, analytical results and the analytical approximation of outage probability in RNRF, NNNF, and NNFF. The outage probability of the near MTC device in NNNF is the same as that of NNFF, which is denoted as NNN(F)F, as shown in Fig. 2(a). In this figure, the outage probabilities of the near MTC device in the three MTC device pairing schemes are given. Outage probabilities of the far MTC device in RNRF, NNNF, and NNFF are presented in Fig. 2(b)–(d), respectively. From these performance evaluation results, the following observations can be made: 1) The analytical results obtained for the RNRF, NNNF, and NNFF schemes match very well with the equivalent results obtained by means of computer simulations; 2) in the high SNR region, the analytical approximations are very tight; 3) the near MTC device in NNN(F)F achieves lower outage probabilities as compared to RNRF.

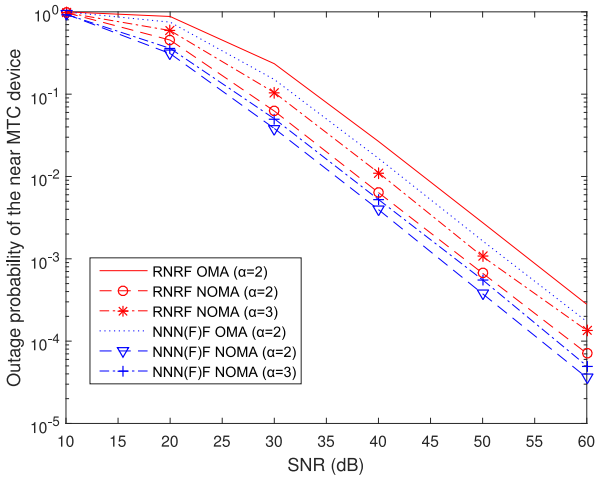

Fig. 3. Outage probability of the near MTC device versus SNR for different values of the path loss exponent.

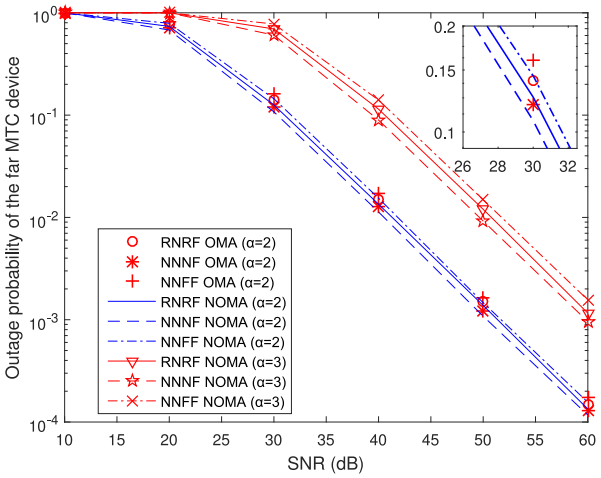

Fig. 4. Outage probability of the far MTC device versus SNR for different values of the path loss exponent.

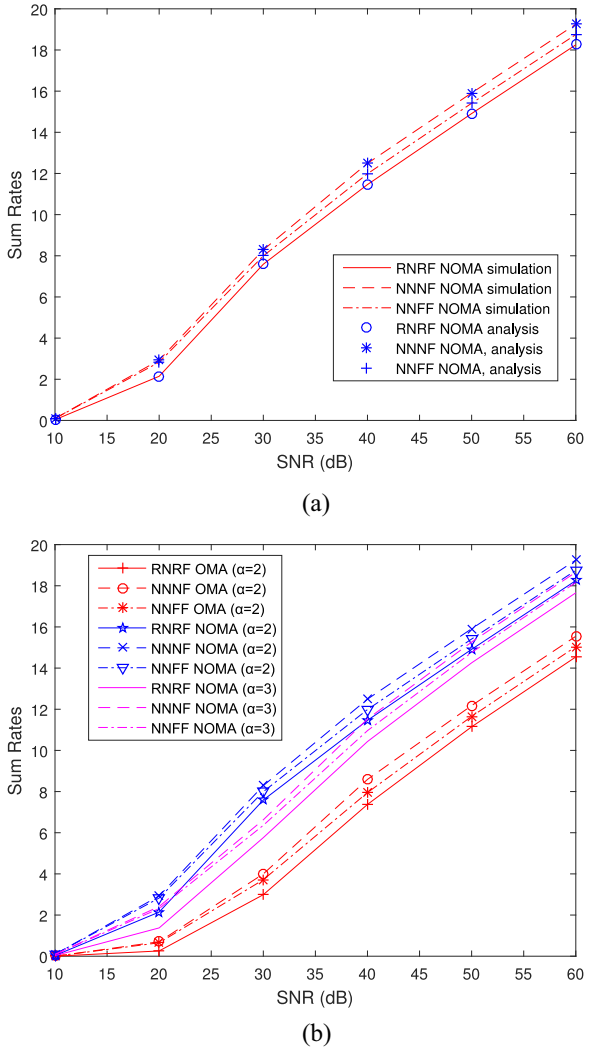

Fig. 5. Sum rate of mmWave-NOMA and mmWave-OMA in the proposed MTC device paring schemes versus SNR. (a) Monte Carlo simulation results and analytical results of outage sum rates versus SNR. (b) Outage sum rates versus SNR, with different path loss exponents.

Fig. 3 plots the outage probability of the near MTC device versus SNR. The outage probability of the near MTC device versus SNR is given for different values of the path loss exponents of RNRF and NNN(F)F, namely $\alpha = 2$ and $\alpha = 3$, respectively. From the performance results shown in Fig. 3, the following observations have been made.

1) The outage probability of the near MTC device in cellular M2M communications with the mmWave-NOMA transmission scheme is better than by using a mmWave-OMA transmission scheme.
2) The outage probability of the near MTC device increases as the path loss exponent increases.
3) Among the three schemes, NNN(F)F achieves the lower outage probability.
4) When the outage probability of RNRF is equal to the outage probability of NNN(F)F, the transmit SNR difference between the two schemes is about 3 dB.

Fig. 4 plots the outage probability of the far MTC device versus SNR. The outage probability of the far MTC device versus SNR is presented for different values of the path loss exponents of RNRF, NNNF, and NNFF. Similar to Fig. 3, the values of the path loss are set as $\alpha = 2$ and $\alpha = 3$, respectively. From Fig. 4, several observations are in order: 1) Again here, the outage probability of the far MTC device in cellular M2M communications with the mmWave-NOMA transmission scheme is better than that with the mmWave-OMA transmission scheme; 2) the outage probability of the far MTC device increases as the path loss exponent increases; and 3) among the three schemes, NNNF achieves the lowest outage probability, and NNFF achieves the highest outage probability.

Fig. 5 illustrates the outage sum rates versus SNR. In Fig. 5(a), Monte Carlo simulation results and the analytical results of outage sum rates in RNRF, NNNF, and NNFF are presented. In Fig. 5(b), outage sum rates as a function of the SNR are shown with different path loss exponents for the three proposed schemes, and the corresponding OMA simulation results are also given as a benchmark when $\alpha = 2$. From these performance results, it is clear that: 1) analytical results of RNRF, NNNF, and NNFF match the simulation

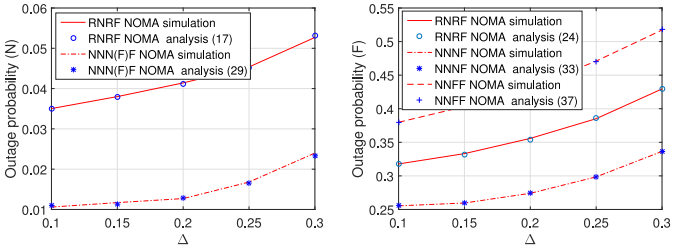

Fig. 6. Outage probability versus Δ. (a) Near MTC device in the three MTC device pairing schemes. (b) Far MTC device in the three MTC device pairing schemes.

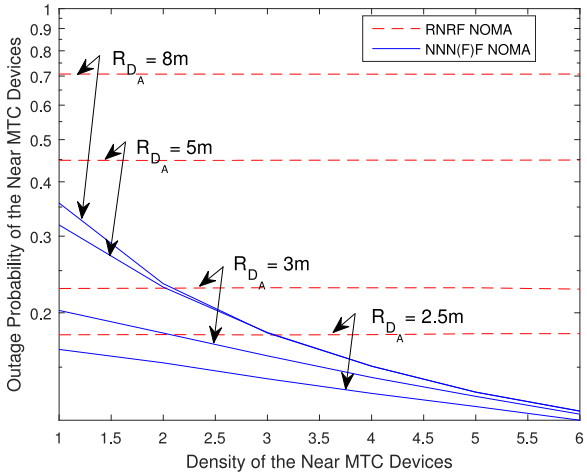

Fig. 7. Outage probability of the near MTC device versus density of the near MTC device with different R_{D_A}, where $R_1 = 2.5$ BPCU, $R_2 = 1$ BPCU, $R_{D_C} = 12$, and $R_{D_B} = 14$.

results well; 2) outage sum rates of cellular M2M communications with the mmWave-NOMA transmission scheme are better than that of cellular M2M communications with the mmWave-OMA transmission scheme; 3) outage sum rates of the schemes decrease as path loss exponent increases; and 4) among the three proposed schemes, the outage sum rates of the NNNF are the best while the outage sum rates of the RNRF are the worst.

Fig. 6 plots the outage probability versus Δ. In Fig. 6(a), the outage probabilities of the near MTC device in the three MTC device pairing schemes are given. In Fig. 6(b), the outage probabilities of the far MTC device in the three MTC device pairing schemes are shown. From these results it can be concluded that, outage probabilities of the near and far MTC devices increase as Δ increases, which means that $\Delta \to 0$ can guarantee a large effective channel gain.

Fig. 7 plots the outage probability of the near MTC device versus density of the near MTC devices with different R_{D_A}. The outage probability of the near MTC device in NNN(F)F decrease as the density of the near MTC devices λ_A increases, because the possibility of scheduling MTC devices with a higher effective channel gain improves. However, outage probability of the near MTC device in RNRF is invariant. This happens because the possibility of scheduling MTC devices with a higher effective channel gain does not change.

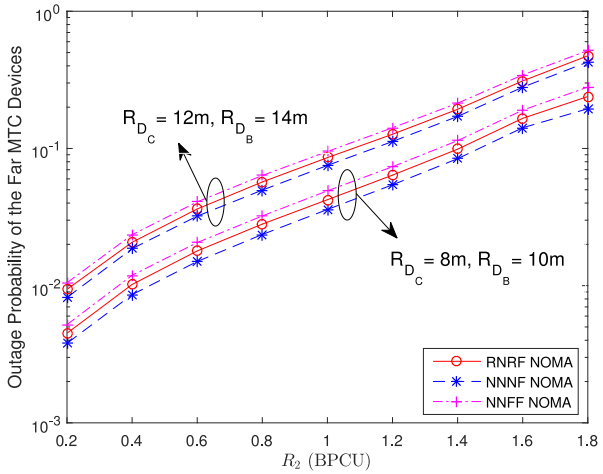

Fig. 8. Outage probability of the far MTC device versus R_2 with different R_{D_C} and R_{D_B} in the three pairing schemes.

Furthermore, the outage probability of RNRF and NNN(F)F decreases as R_{D_A} decreases, since the path loss of the near MTC devices becomes smaller with the decreasing radius.

Fig. 8 illustrates the outage probability of the far MTC device versus R_2 with different R_{D_C} and R_{D_B} for the three proposed pairing schemes. It is noted that the outage probability of the far MTC device in RNRF, NNNF, and NNFF increase as R_2 increases, since the QoS of MTC devices becomes higher with the increasing R_2. Moreover, outage probabilities of RNRF, NNNF, and NNFF increase as R_{D_C} and R_{D_B} increase, because the path loss of the near MTC devices becomes larger with the increasing radius.

V. Conclusion

In this paper, a new mmWave-NOMA transmission scheme in cellular M2M communications for IoT which can meet the QoS offered to MTC devices, has been introduced and its performance has been analyzed. Based on the distinct advantages of the proposed mmWave-NOMA transmission scheme, massive connectivity of IoT can be achieved in cellular M2M communications. Using the distance between the MTC devices and the BS as a selection criterion, we have proposed three different MTC device pairing schemes which can reduce latency and system overhead, and have focused on a single beam, employing random beamforming. Theoretical studies have shown that, among the proposed three schemes, the outage probability of the near MTC device of NNN(F)F is lower than that of the near MTC device of RNRF. Regarding the outage probability of the far MTC device, NNNF and NNFF achieve the best and worst performance, respectively. These theoretical results have been validated by complementary performance evaluation results obtained by means of Monte Carlo computer simulations.

References

[1] A. Al-Fuqaha, M. Guizani, M. Mohammadi, M. Aledhari, and M. Ayyash, "Internet of Things: A survey on enabling technologies, protocols, and applications," *IEEE Commun. Surveys Tuts.*, vol. 17, no. 4, pp. 2347–2376, 4th Quart., 2015.

[2] D. Singh, G. Tripathi, and A. J. Jara, "A survey of Internet-of-Things: Future vision, architecture, challenges and services," in *Proc. IEEE World Forum Internet Things (WF-IoT)*, Seoul, South Korea, Mar. 2014, pp. 287–292.

[3] A. Zanella, N. Bui, A. Castellani, L. Vangelista, and M. Zorzi, "Internet of Things for smart cities," *IEEE Internet Things J.*, vol. 1, no. 1, pp. 22–32, Feb. 2014.

[4] J. A. Stankovic, "Research directions for the Internet of Things," *IEEE Internet Things J.*, vol. 1, no. 1, pp. 3–9, Feb. 2014.

[5] S. Li *et al.*, "Joint admission control and resource allocation in edge computing for Internet of Things," *IEEE Netw.*, vol. 32, no. 1, pp. 72–79, Jan./Feb. 2018.

[6] G. Wunder *et al.*, "5GNOW: Non-orthogonal, asynchronous waveforms for future mobile applications," *IEEE Commun. Mag.*, vol. 52, no. 2, pp. 97–105, Feb. 2014.

[7] J. Suomalainen, "Smartphone assisted security pairings for the Internet of Things," in *Proc. Wireless Commun. Veh. Technol. Inf. Theory Aerosp. Electron. Syst. (VITAE)*, Aalborg, Denmark, May 2014, pp. 1–5.

[8] L. Atzori, A. Iera, and G. Morabito, "The Internet of Things: A survey," *Comput. Netw.*, vol. 54, no. 15, pp. 2787–2805, Oct. 2010.

[9] X. Liu and N. Ansari, "Green relay assisted D2D communications with dual battery for IoT," in *Proc. IEEE Glob. Commun. Conf. (GLOBECOM)*, Washington, DC, USA, Dec. 2016, pp. 1–6.

[10] S. Lin *et al.*, "Advanced dynamic channel access strategy in spectrum sharing 5G systems," *IEEE Wireless Commun.*, vol. 24, no. 5, pp. 74–80, Oct. 2017.

[11] Y. Liu, Z. Qin, M. Elkashlan, Y. Gao, and L. Hanzo, "Enhancing the physical layer security of non-orthogonal multiple access in large-scale networks," *IEEE Trans. Wireless Commun.*, vol. 16, no. 3, pp. 1656–1672, Mar. 2017.

[12] Z. Yang, W. Xu, Y. Pan, C. Pan, and M. Chen, "Energy efficient resource allocation in machine-to-machine communications with multiple access and energy harvesting for IoT," *IEEE Internet Things J.*, vol. 5, no. 1, pp. 229–245, Feb. 2018.

[13] M. Shirvanimoghaddam, M. Dohler, and S. J. Johnson, "Massive non-orthogonal multiple access for cellular IoT: Potentials and limitations," *IEEE Commun. Mag.*, vol. 55, no. 9, pp. 55–61, Sep. 2017.

[14] S.-Y. Lien, K.-C. Chen, and Y. Lin, "Toward ubiquitous massive accesses in 3GPP machine-to-machine communications," *IEEE Commun. Mag.*, vol. 49, no. 4, pp. 66–74, Apr. 2011.

[15] M. Shirvanimoghaddam, M. Condoluci, M. Dohler, and S. J. Johnson, "On the fundamental limits of random non-orthogonal multiple access in cellular massive IoT," *IEEE J. Sel. Areas Commun.*, vol. 35, no. 10, pp. 2238–2252, Oct. 2017.

[16] K. Higuchi and A. Benjebbour, "Non-orthogonal multiple access (NOMA) with successive interference cancellation for future radio access," *IEICE Trans. Commun.*, vol. 98, no. 3, pp. 403–414, Mar. 2015.

[17] K. Higuchi and Y. Kishiyama, "Non-orthogonal access with random beamforming and intra-beam SIC for cellular MIMO downlink," in *Proc. IEEE Veh. Technol. Conf. (VTC Fall)*, Las Vegas, NV, USA, Sep. 2013, pp. 1–5.

[18] Z. Ding, L. Dai, R. Schober, and H. V. Poor, "NOMA meets finite resolution analog beamforming in massive MIMO and millimeter-wave networks," *IEEE Commun. Lett.*, vol. 21, no. 8, pp. 1879–1882, Aug. 2017.

[19] Y. Liu *et al.*, "Nonorthogonal multiple access for 5G and beyond," *Proc. IEEE*, vol. 105, no. 12, pp. 2347–2381, Dec. 2017.

[20] M. F. Kader, M. B. Shahab, and S. Y. Shin, "Exploiting non-orthogonal multiple access in cooperative relay sharing," *IEEE Commun. Lett.*, vol. 21, no. 5, pp. 1159–1162, May 2017.

[21] S. Timotheou and I. Krikidis, "Fairness for non-orthogonal multiple access in 5G systems," *IEEE Signal Process. Lett.*, vol. 22, no. 10, pp. 1647–1651, Oct. 2015.

[22] Y. Liu, M. Elkashlan, Z. Ding, and G. K. Karagiannidis, "Fairness of user clustering in MIMO non-orthogonal multiple access systems," *IEEE Commun. Lett.*, vol. 20, no. 7, pp. 1465–1468, Jul. 2016.

[23] S. M. R. Islam, N. Avazov, O. A. Dobre, and K.-S. Kwak, "Power-domain non-orthogonal multiple access (NOMA) in 5G systems: Potentials and challenges," *IEEE Commun. Surveys Tuts.*, vol. 19, no. 2, pp. 721–742, 2nd Quart., 2017.

[24] Z. Ding, F. Adachi, and H. V. Poor, "The application of MIMO to non-orthogonal multiple access," *IEEE Trans. Wireless Commun.*, vol. 15, no. 1, pp. 537–552, Jan. 2016.

[25] Y. Liu, Z. Qin, M. Elkashlan, A. Nallanathan, and J. A. McCann, "Non-orthogonal multiple access in large-scale heterogeneous networks," *IEEE J. Sel. Areas Commun.*, vol. 35, no. 12, pp. 2667–2680, Dec. 2017.

[26] Z. Ding *et al.*, "A survey on non-orthogonal multiple access for 5G networks: Research challenges and future trends," *IEEE J. Sel. Areas Commun.*, vol. 35, no. 10, pp. 2181–2195, Oct. 2017.

[27] Z. Ding, P. Fan, and V. Poor, "Impact of user pairing on 5G non-orthogonal multiple access downlink transmissions," *IEEE Trans. Veh. Technol.*, vol. 65, no. 8, pp. 6010–6023, Aug. 2016.

[28] B. Kim *et al.*, "Non-orthogonal multiple access in a downlink multiuser beamforming system," in *Proc. IEEE Mil. Commun. Conf. (MILCOM)*, San Diego, CA, USA, Nov. 2013, pp. 1278–1283.

[29] S. Liu, C. Zhang, and G. Lyu, "User selection and power schedule for downlink non-orthogonal multiple access (NOMA) system," in *Proc. IEEE Int. Conf. Commun. Workshop (ICCW)*, London, U.K., Jun. 2015, pp. 2561–2565.

[30] B. Kim *et al.*, "Uplink NOMA with multi-antenna," in *Proc. IEEE Veh. Technol. Conf. (VTC Spring)*, Glasgow, U.K., May 2015, pp. 1–5.

[31] J. Kim, J. Koh, J. Kang, K. Lee, and J. Kang, "Design of user clustering and precoding for downlink non-orthogonal multiple access (NOMA)," in *Proc. IEEE Mil. Commun. Conf. (MILCOM)*, Tampa, FL, USA, Oct. 2015, pp. 1170–1175.

[32] Z. Zhang *et al.*, "Non-orthogonal multiple access for cooperative multicast millimeter wave wireless networks," *IEEE J. Sel. Areas Commun.*, vol. 35, no. 8, pp. 1794–1808, Aug. 2017.

[33] A. S. Marcano and H. L. Christiansen, "Performance of non-orthogonal multiple access (NOMA) in mmWave wireless communications for 5G networks," in *Proc. Comput. Netw. Commun. (ICNC)*, Santa Clara, CA, USA, Jan. 2017, pp. 969–974.

[34] Z. Ding, P. Fan, and H. V. Poor, "Random beamforming in millimeter-wave NOMA networks," *IEEE Access*, vol. 5, pp. 7667–7681, 2017.

[35] L. Kong, M. K. Khan, F. Wu, G. Chen, and P. Zeng, "Millimeter-wave wireless communications for IoT-cloud supported autonomous vehicles: Overview, design, and challenges," *IEEE Commun. Mag.*, vol. 55, no. 1, pp. 62–68, Jan. 2017.

[36] Z. Ding, L. Dai, and H. V. Poor, "MIMO-NOMA design for small packet transmission in the Internet of Things," *IEEE Access*, vol. 4, pp. 1393–1405, 2016.

[37] H. Sun, Q. Wang, S. Ahmed, and R. Q. Hu, "Non-orthogonal multiple access in a mmWave based IoT wireless system with SWIPT," in *Proc. Veh. Technol. Conf. (VTC Spring)*, Sydney, NSW, Australia, Jun. 2017, pp. 1–5.

[38] Z. Yang, W. Xu, H. Xu, J. Shi, and M. Chen, "Energy efficient non-orthogonal multiple access for machine-to-machine communications," *IEEE Commun. Lett.*, vol. 21, no. 4, pp. 817–820, Apr. 2017.

[39] G. Lee, Y. Sung, and J. Seo, "Randomly-directional beamforming in millimeter-wave multiuser MISO downlink," *IEEE Trans. Wireless Commun.*, vol. 15, no. 2, pp. 1086–1100, Feb. 2016.

[40] Y. Liu, Z. Ding, M. Elkashlan, and H. V. Poor, "Cooperative non-orthogonal multiple access with simultaneous wireless information and power transfer," *IEEE J. Sel. Areas Commun.*, vol. 34, no. 4, pp. 938–953, Apr. 2016.

Tiejun Lv (M'08–SM'12) received the M.S. and Ph.D. degrees in electronic engineering from the University of Electronic Science and Technology of China, Chengdu, China, in 1997 and 2000, respectively.

From 2001 to 2003, he was a Post-Doctoral Fellow with Tsinghua University, Beijing, China. In 2005, he was a Full Professor with the School of Information and Communication Engineering, Beijing University of Posts and Telecommunications. From 2008 to 2009, he was a Visiting Professor with the Department of Electrical Engineering, Stanford University, Stanford, CA, USA. He has authored over 50 IEEE journal papers and 170 conference papers on the physical layer of wireless mobile communications. His current research interests include signal processing, communications theory and networking.

Dr. Lv was a recipient of the Program for New Century Excellent Talents in University Award from the Ministry of Education, China, in 2006 and the Nature Science Award in the Ministry of Education of China for the hierarchical cooperative communication theory and technologies in 2015.

Yuyu Ma received the B.Eng. degree from the Xi'an University of Posts and Telecommunications, Xi'an, China, in 2015. She is currently pursuing the M.S. degree at the Beijing University of Posts and Telecommunications, Beijing, China.

Her current research interests include nonorthogonal multiple access, cooperative communications, and Internet of Things.

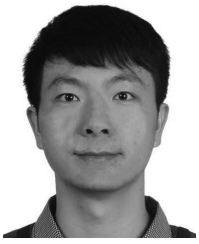

Jie Zeng (M'09–SM'16) received the B.S. and M.S. degrees in electronic engineering from Tsinghua University, Beijing, China, in 2006 and 2009, respectively.

He has authored or co-authored 3 books and over 100 conference and journal papers. He holds over 20 Chinese and 5 international patents. His current research interests include novel network architecture, ultradense networks, and novel multiple access.

Mr. Zeng was a recipient of the Science and Technology Award of Beijing in 2015 and the Best Cooperation Award of Samsung Electronics in 2016.

P. Takis Mathiopoulos (SM'94) received the Ph.D. degree in digital communications from the University of Ottawa, Ottawa, ON, Canada, in 1989.

From 1982 to 1986, he was with Raytheon Canada Ltd., involved in the areas of air navigational and satellite communications. In 1989, he joined as an Assistant Professor the Department of Electrical and Computer Engineering, The University of British Columbia (UBC), Vancouver, BC, Canada, where he was a faculty member until 2003, holding the rank of Professor from 2000 to 2003. From 2000 to 2014, he was the Director, from 2000 to 2005, and then the Director of Research of the Institute for Space Applications and Remote Sensing (ISARS), National Observatory of Athens, where he established the Wireless Communications Research Group. From 2000 to 2004, as the ISARS Director, he led the institute to a significant expansion R&D growth, and international scientific recognition. For these achievements, ISARS has been selected as the National Centre of Excellence from 2005 to 2008. Since 2014, he has been a Professor of telecommunications with the Department of Informatics and Telecommunications, National and Kapodistrian University of Athens, Athens, Greece. From 2008 to 2013, he was appointed as a Guest Professor by Southwest Jiaotong University, Chengdu, China. He has been appointed by the Government of China as a Senior Foreign Expert with the School of Information Engineering, Yangzhou University, Yangzhou, China, from 2014 to 2017, and by Keio University, as a Guest Professor (Global) with the Graduate School of Science and Technology, from 2015 to 2016 and from 2017 to 2018, under the Top Global University Project of the Ministry of Education, Culture, Sports, Science and Technology, Government of Japan. For the last 25 years, he has been conducting research mainly on the physical layer of digital communication systems for terrestrial and satellite applications, and also in the fields of remote sensing and the Internet of Things. In these areas, he has co-authored over 120 journal papers published mainly in various IEEE journals, 1 book (edited), 5 book chapters, and over 140 conference papers. He has been or currently serves on the Editorial Board of several archival journals, including the *IET Communications* and the IEEE TRANSACTIONS ON COMMUNICATIONS from 1993 to 2005.

Dr. Mathiopoulos has regularly served as a consultant for various governmental and private organizations. Since 1993, he has served on a regular basis as a Scientific Advisor and a Technical Expert for the European Commission (EC). From 2001 to 2014, he has served as a Greek Representative to high-level committees in the EC and the European Space Agency. He has been a member of the Technical Program Committees (TPC) of more than 70 international IEEE conferences, and also the TPC Vice Chair for the 2006-S IEEE Vehicular Technology Conference (VTC) and the 2008-F IEEE VTC, the Co-Chair of International Conference on Future Information Technology 2011, and the AUTOMOTIVE17. He has delivered numerous invited presentations, including plenary and keynote lectures, and has taught many short courses all over the world. As a faculty member UBC, he has been awarded an Advanced Systems Institute Fellowship and also a Killam Research Fellowship. He was a co-recipient of two best conference paper awards. He is the recipient of the 2017 Satellite and Space Communications Distinguished Service Award of the IEEE Communications Society presented to him for his outstanding contributions to the satellite and space international scientific community.